method (Hill and Wait, 1980) which has been used for calculations of ground-wave propagation over sea ice (Hill and Wait, 1981b).

In the case of HF ground-wave propagation over sea ice, a trapped surface wave (Hill and Wait, 1981b) was supported because of the highly inductive surface impedance. As seen in Table 2, a layer of snow over ground does not produce a phase angle of Δ much larger than 45°. Consequently, the main effect of the snow layer is to increase the magnitude of Δ and to decrease the ground-wave field strength. For small depths the effect is small, but for depths of packed snow on the order of a meter the effect becomes significant. As seen in Figure 8, the effect is more prominent at the higher frequencies.

6. SPECIFIC PATH CALCULATIONS

In this section we apply program WAGSLAB to several paths. The smooth paths in the Netherlands are a good check on WAGSLAB because the exact residue series solution for a spherical earth (Hill and Wait, 1980) is available as a check. Both earth curvature and atmospheric refraction are included in WAGSLAB by inputting the appropriate earth radius. In all cases, we used the 4/3 earth radius value ($a \approx 8500$ km) to account for normal atmospheric refraction (Bremmer, 1949; Wait, 1962), but other values could be used for different atmospheric conditions.

The irregular, forested terrain in southern West Germany presents a greater challenge to the integral equation approach. We have no experimental results as checks for these paths, but reciprocity provides a good theoretical check. Also, we have found that the multiple knife-edge model of Vogler (1981) is in reasonably good agreement with the integral equation solution for long, rough paths.

6.1 Smooth Paths in the Netherlands

Measurements of field strength and bit error rate have recently been carried out on paths of 60 km and 80 km in the Netherlands (Van der Vis, 1979). The frequencies range from 2 MHz to 30 MHz, and both vertical and horizontal polarization were transmitted and received. Both paths had the same transmitter, and the two paths were nearly in line. An examination of topographic maps of the area revealed that both paths were over very smooth (less than a few meters in elevation change), unforested terrain with no cities. The main feature of interest was a section of low ground conductivity (dry, sandy soil) at the end of the 80 km path. Consequently, we modeled the path with two smooth sections as shown in Figure 9. Unfortunately, no ground conductivity measurements were made, but we assume the values suggested by Van der Vis (1979): $\varepsilon_g = 15$ and $\sigma_g = 10^{-2}$ S/m for the first

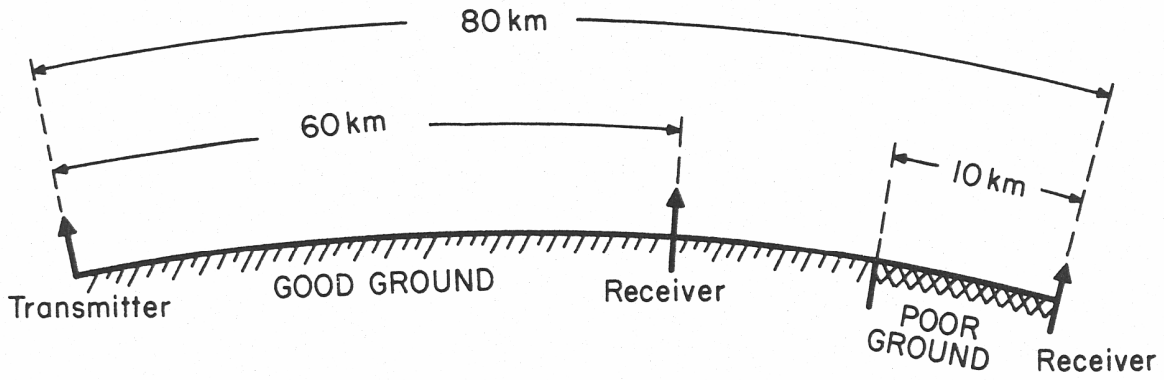

Figure 9. Smooth path in the Netherlands with receiving sites at 60 km and 80 km. The first 70 km has good ground (ε_g = 15 and σ_g = 10^{-2} S/m), and the last 10 km has poor ground (ε_g = 3 and σ_g = 10^{-4} S/m).

70 km of good ground and ε_g=3 and σ_g=10^{-4} S/m for the remaining section of poor ground.

In Figures 10-12, we show the magnitude of the attenuation function f along the path for three different frequencies. As usual, the attenuation function is defined as the ratio of the vertical electric field to that over flat, perfectly conducting ground. Both the transmitting and receiving antennas are assumed to be located at the surface, and the measured data are adjusted to account for the antenna heights by assuming the height-gain function in (13). In each case the integral equation result shows a rapid drop in field strength beyond 70 km because of the decrease in ground constants. The measured data are consistent with this drop, but a detailed comparison is not possible because measurements are available only at 60 km and 80 km. It appears that the ground conductivity and dielectric constant which were suggested by Van der Vis (1979) for the first 70 km were a little too high. Lower values would have provided a better fit with the measurements.

For comparison in Figures 10-12, we also show the spherical earth and flat earth results for a uniform path (Hill and Wait, 1980). Because the integral equation solution assumes no backscatter, it should agree with the spherical earth theory over the first 70 km. The accuracy of the integral equation solution becomes

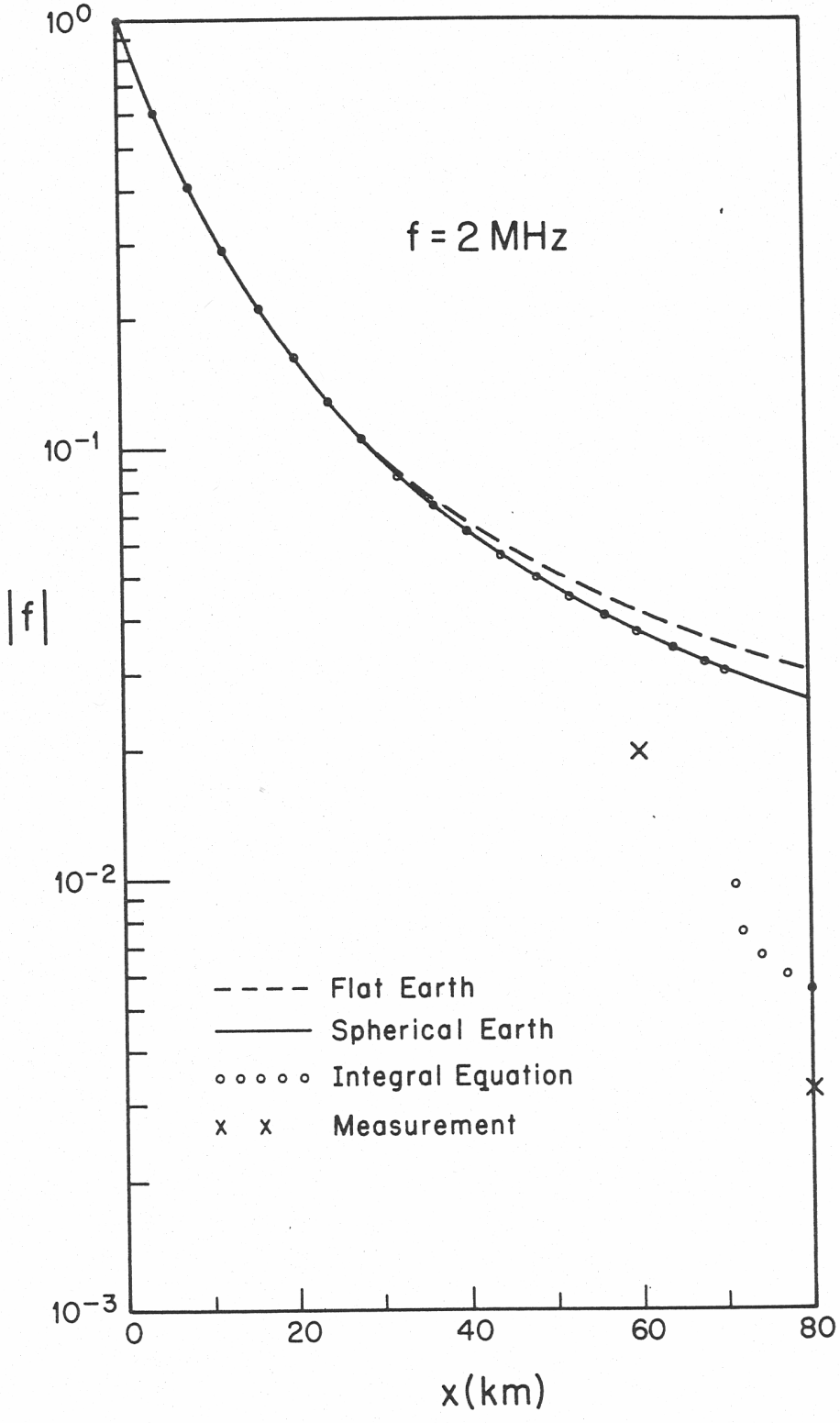

Figure 10. Comparison of measurement with three theories at 2 MHz for a smooth path in the Netherlands. Only the integral equation solution takes into account the poor ground section shown in Figure 9.

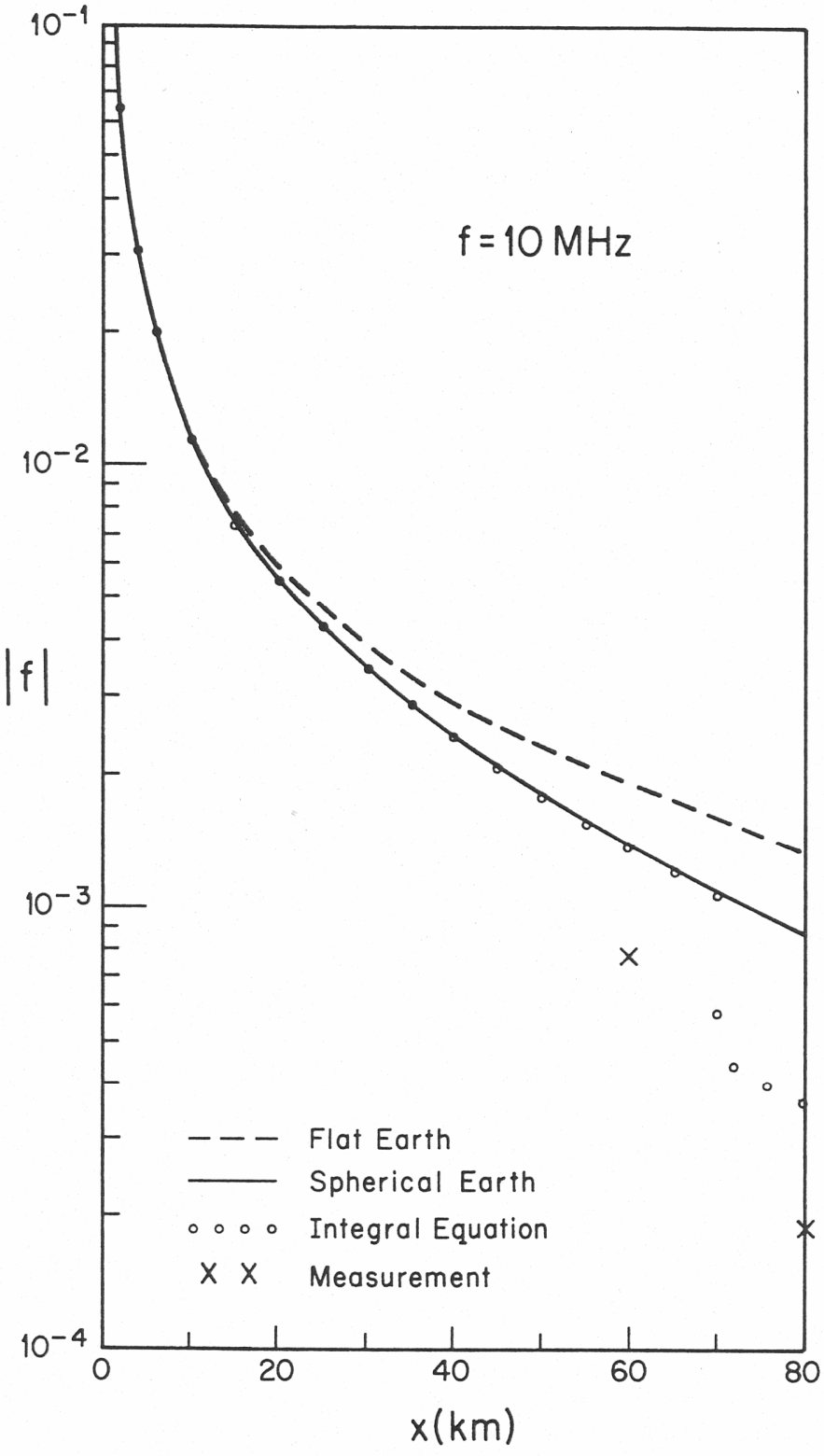

Figure 11. Comparison of measurement with three theories at 10 MHz for a smooth path in the Netherlands. Only the integral equation solution takes into account the poor ground section shown in Figure 9.

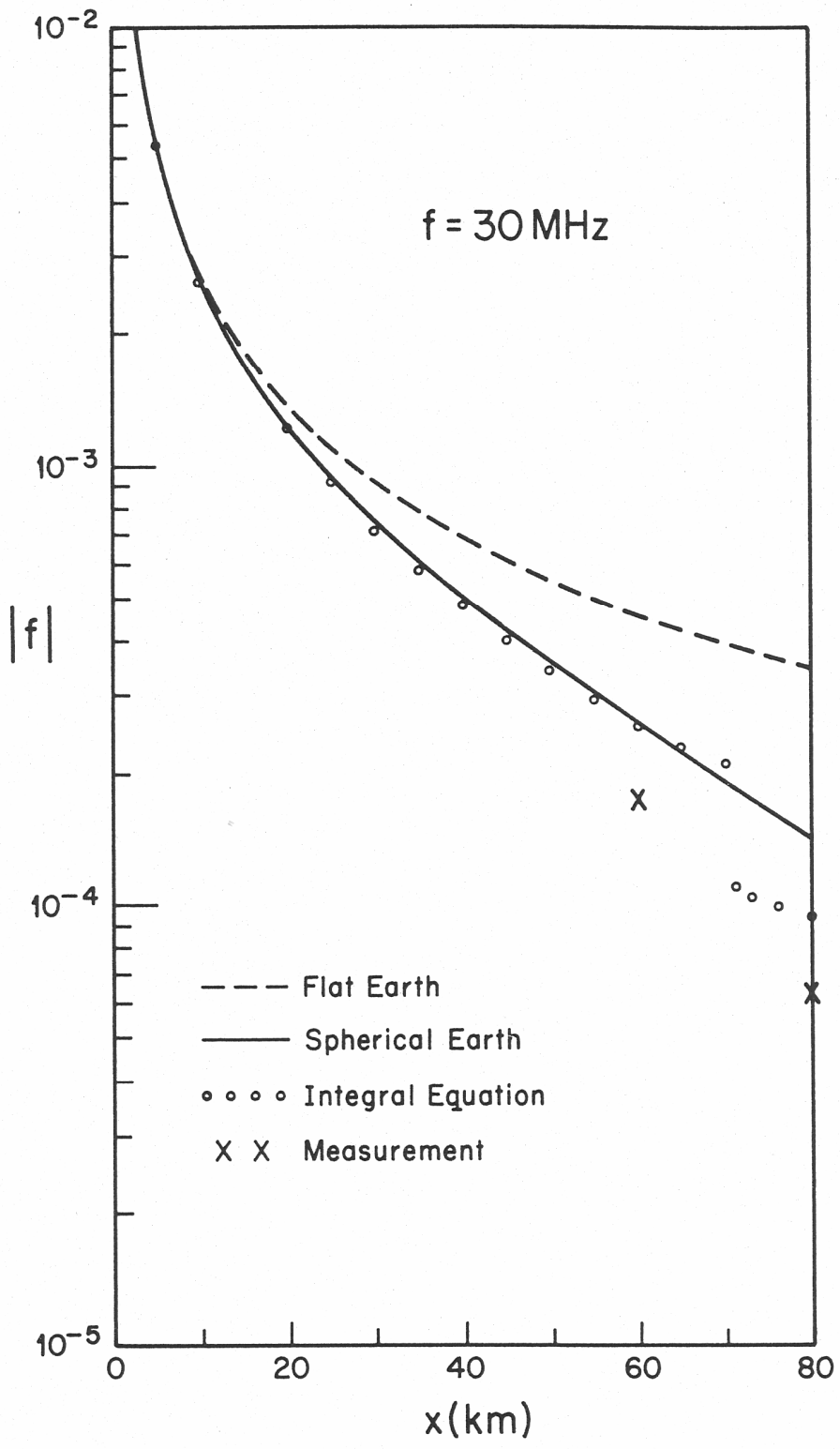

Figure 12. Comparison of measurement with three theories at 30 MHz for a smooth path in the Netherlands. Only the integral equation solution takes into account the poor ground section shown in Figure 9.

harder to maintain at higher frequencies and longer paths. At 30 MHz, it was necessary to sample approximately every 40 m (equals 4 wavelengths) along the path to obtain the agreement (which is not perfect) in Figure 12. This resulted in 2000 sample points along the path and an execution time of approximately 15 min on a large mainframe computer. This rather long run time decreases rapidly as the frequency is decreased as indicated by (25). Thus program WAGSLAB can be considered very efficient for the lower portion of the HF band but only marginally efficient at 30 MHz. It should probably not be used above 30 MHz except for very short paths.

Also shown for comparison in Figures 10-12 is the flat earth result for a uniform path. It is easy to see that earth curvature is not particularly important at 2 MHz but is quite important at 30 MHz. An approximate upper bound in path length and frequency for the validity of flat earth theory can be obtained from examining the spherical earth theory. The earth curvature can normally be neglected when the following inequality is satisfied

$$\left(\frac{ka}{2}\right)^{1/3} \left(\frac{x}{a}\right) \ll 1 \quad . \tag{48}$$

From examination of numerical results (Hill and Wait, 1980), we can set the right-hand side of (48) equal to 0.2. If we assume a = 8500 km (= 4/3 earth radius), then the maximum path length x_{max} for good agreement between flat and spherical earth theory is given by

$$x_{max} \simeq \frac{38.1}{f_{MHz}^{1/3}} \text{ (km)} \quad , \tag{49}$$

where f_{MHz} is the frequency in megahertz. From (49), x_{max} = 30.2 km at 2 MHz, and x_{max} = 12.3 km at 30 MHz. For x greater than x_{max}, the flat earth theory predicts a field strength which is too high as seen in Figures 10-12. For example, in Figure 12 at a frequency of 30 MHz and a distance of 80 km, the flat earth field strength is a factor of 2.43 greater (= 7.7 dB) than the spherical earth result.

6.2 Irregular, Forested Terrain in West Germany

In order to provide a more demanding test for program WAGSLAB, we examined two paths over irregular, forested terrain in southern West Germany. We have no experimental data for these paths at this time, but there has been some planning for future HF ground wave measurements in the area (NTIA Technical Memorandum 82-80 by Kissick and Adams, limited distribution).

The path which we considered in most detail is a 56.6 km path from Inneringen to Boblingen. The terrain profile shown in Figure 13 was generated from the files of the Defense Mapping Agency. The terrain profile checks very well with the profile which we obtained by hand from 1:50,000 scale maps of the area. The path contains numerous forested sections and three short sections with buildings. For the forested sections, we chose a height D of 20 m and the "average" electrical properties of Table 1. For the urban areas we did not have available information on building height and density. We chose a building height D of 10 m and a building density B of 0.2 (Causebrook, 1978a). From (47), this yields dielectric constants of $\varepsilon_v=\varepsilon_h=1.82$. For conductivity we took the value for "thin" forest, $\sigma_v=\sigma_h=3 \times 10^{-5}$ S/m, rather than $\sigma_v=\sigma_h=0$ as given by (47) because it seems likely that some trees are present in the urban areas. The actual locations of the forest and urban slabs are given by the input data in the sample computer run in Appendix C. We also had to guess at the ground parameters and chose the following values for fairly good ground over the entire path: $\varepsilon_g=10$ and $\sigma_g=10^{-2}$ S/m.

In Figures 14-18, we show propagation from Inneringen to Boblingen both with and without the forest and building slabs at five frequencies from 2 MHz to 30 MHz. In all cases, both the transmitting and receiving antennas are located at the surface of the ground ($h_a=h_r=-D$). As a result, the dotted curves which include the slabs are more irregular because the height-gain function $G(h_r)$ is discontinuous as the receiving antenna moves from bare ground into a slab. This results in a discontinuous value of f_h which is proportional to $G(h_r)$ as shown by (21). The dependence of G on height both in and above the forest slab is shown in Figure 19. In most cases, $|G(h_r)|$ is less than unity in the slab and increases from unity above the slab.

The height-gain effect can be considered a local effect on the field, but the normalized surface impedance $\Delta(\xi)$ influences the field at all points for $x > \xi$ as seen by (20). In most cases, $|\Delta|$ is greater in the forest region than over bare ground. Consequently, the dotted curves in Figures 14-18 which include the forest and urban slabs generally lie below the solid curves for bare ground. At the higher frequencies where the terrain roughness is more important, the effect of the slabs is less dominant. The analytical solution for a spherical earth (Hill and Wait, 1981b) is shown in Figure 20 for both bare ground and forest slab cover. The forest cover has a large effect at 5 MHz, but a much smaller effect at 20 MHz and 30 MHz where diffraction loss becomes important.

Two difficulties with the integral equation approach are that computation time becomes large for long, rough paths at high frequencies as indicated by (25) and

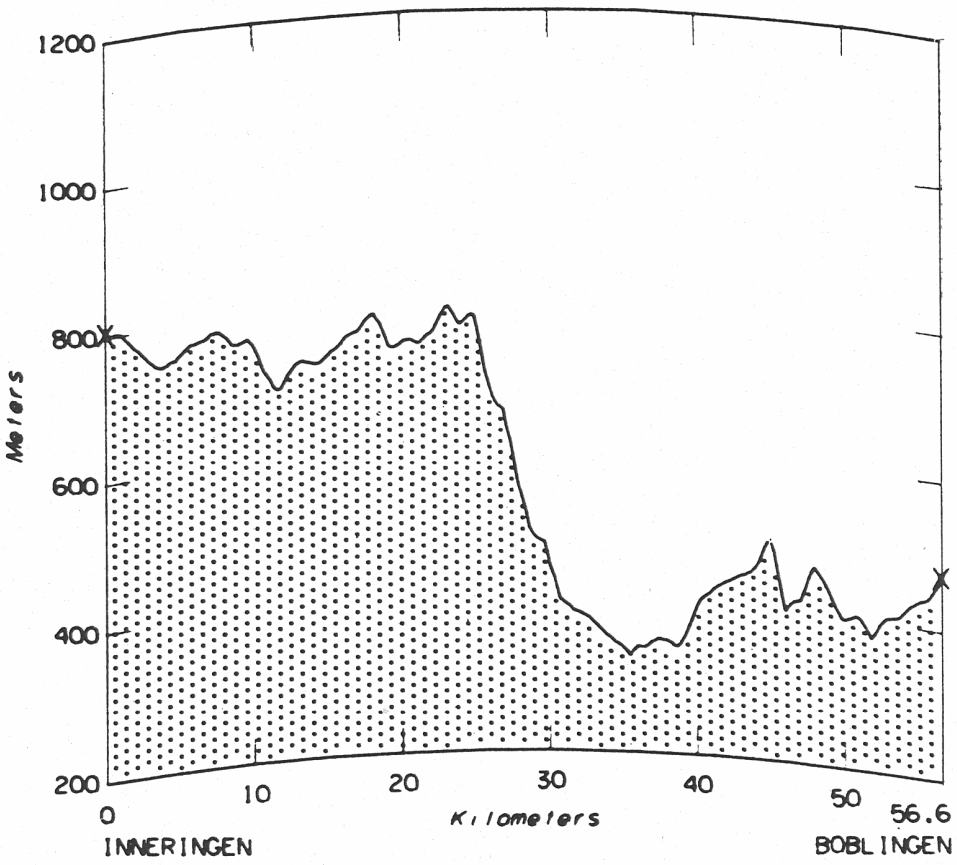

Figure 13. Terrain profile for the path from Inneringen to Boblingen.

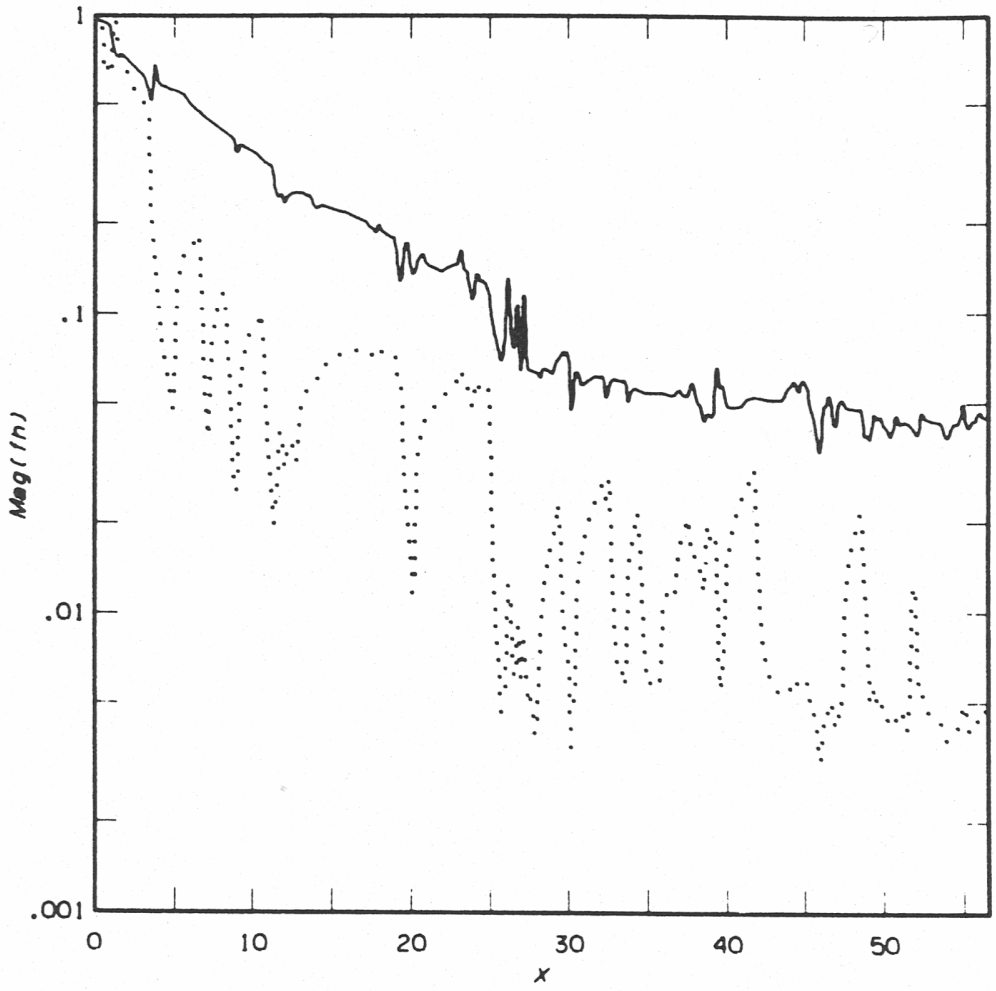

Figure 14. Propagation from Inneringen to Boblingen at 2 MHz. The solid curve is for bare ground, and the dotted curve includes the forest and urban slabs.

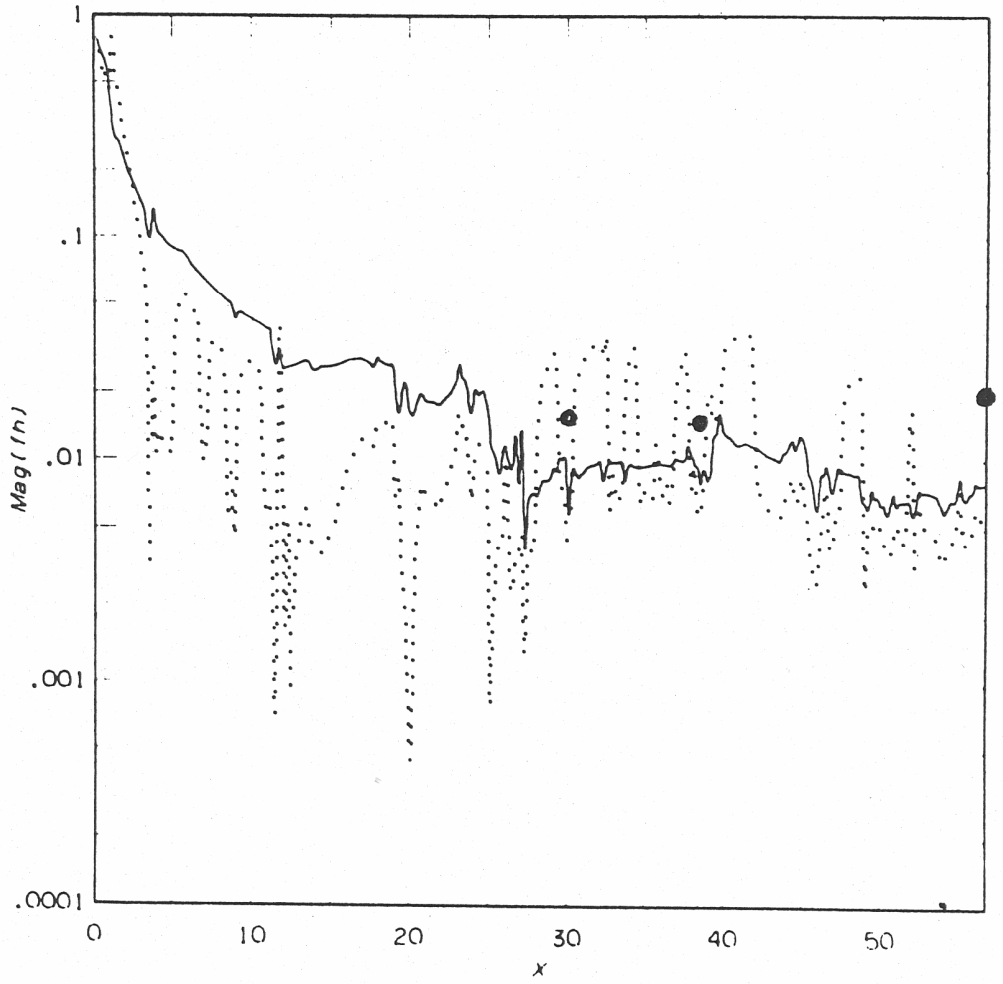

Figure 15. Propagation from Inneringen to Boblingen at 5 MHz. The solid curve is for bare ground, and the dotted curve includes the forest and urban slabs. The circles are obtained from multiple knife-edge diffraction theory.

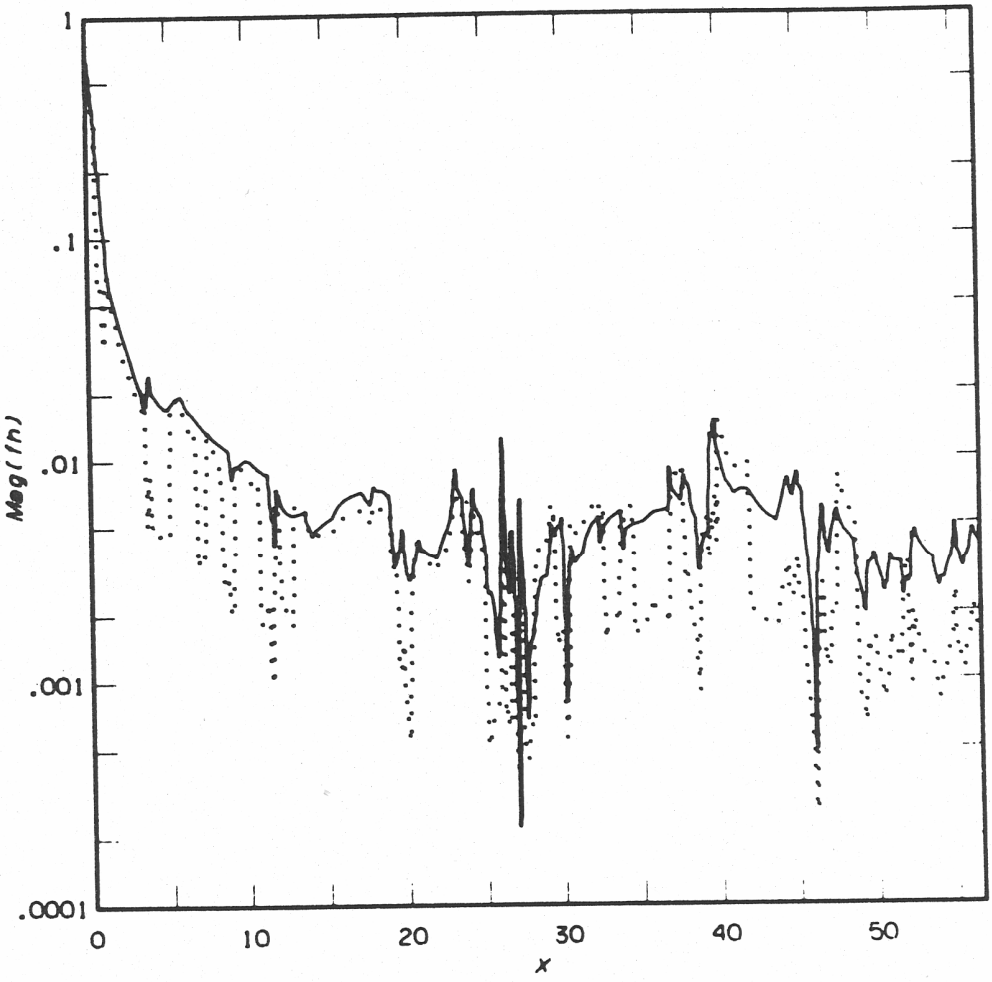

Figure 16. Propagation from Inneringen to Boblingen at 10 MHz. The solid curve is for bare ground, and the dotted curve includes the forest and urban slabs.